Real-Time State-of-Health Estimation of Lithium-Ion Batteries Based on the Equivalent Internal Resistance

XIAOJUN TAN [ID], YUQING TAN [ID], DI ZHAN [ID], ZE YU [ID], YUQIAN FAN [ID], JIANZHI QIU [ID], AND JUN LI [ID]

School of Intelligent Systems Engineering, Sun Yat-sen University, Guangzhou 510275, China

Corresponding author: Jun Li (lijun255@mail.sysu.edu.cn)

ABSTRACT Real-time state-of-health (SoH) estimation is often difficult to obtain due to the unavailability of capacity measurements in real-time monitoring. The equivalent internal resistance (EIR), which is easily obtained and closely related to battery deterioration, is studied as a possible solution for achieving real-time and reliable SoH estimation for lithium-ion batteries. A novel real-time SoH estimation method based on the EIR is introduced for lithium-ion batteries. First, an experimental study of the relationship between the EIR and battery degradation is implemented, and this study is used to develop an empirical description of battery degradation using the EIR vector. Second, a fast extraction method for identifying the EIR in real time is proposed by leveraging the relationship between the EIR vector and state of charge (SoC). Third, a support vector regression (SVR)-based method for real-time SoH estimation is introduced by characterizing the hidden relationship between the EIR vector and battery SoH. The proposed method is demonstrated using laboratory test data. The results show that the proposed method can predict the battery SoH in real time with good accuracy and robustness.

NOMENCLATURE
ABBREVIATIONS

SoH	State-of-Health
EIR	equivalent internal resistance
SoC	State of Charge
SVR	support vector regression
OCV	open circuit voltage
IC	incremental capacity
DV	differential voltage
DTV	differential thermal voltammetry
TIEDVD	time interval of equal discharging voltage difference
UPF	unscented particle filter
BMS	battery management system

GP-ICE	Gaussian process regression for in situ capacity estimation
DoD	Depth Of Discharge
MAE	the mean absolute error
RMSE	the root mean square error
EV	Electric vehicle

SYMBOLS

S_{cap}	the capacity ratio
C_{now}	the current maximum capacity of the battery
C_{rated}	the battery rated capacity
S_R	the internal resistance ratio
R_{EOL}	the internal resistance at the end of battery life
R	the current internal resistance of the battery
R_{new}	the internal resistance of the new battery

The associate editor coordinating the review of this manuscript and approving it for publication was Xiaosong Hu [ID].

R	a set of equivalent internal resistances
$U_{1i}(SoC)$, $U_{2i}(SoC)$, $R_i(SoC)$	the voltage at the last second of charging, the voltage at the last second of shelving and the equivalent internal resistance as the function of SoC in the ***ith*** internal resistance evaluation
I_{ci}, t_i, τ	the charging current, the charging process time and the current second of the charging process in the ***ith*** internal resistance evaluation
R_{1j}, R_{2j}, R_{3j}	the increase of equivalent internal resistance corresponding to SoC of 0.6, 0.7 and 0.8 in the ***ith*** internal resistance evaluation
C	the penalty coefficient of the loss function of SVR model
γ	hyperparameter gamma in SVR model
$U'_{1i}, U'_{2i}, I'_{ci}, R'_i, SoC'$	the charging open-circuit voltage vector, the charging working voltage vector, the current, the equivalent internal resistance vector and the state of charge in the ***ith*** internal resistance evaluation with measurement error
e_{1i}, e_{2i}, e_{3i}	the measurement error of the charging open-circuit voltage, the charging working voltage and the current

I. INTRODUCTION

The degradation of lithium-ion batteries is a complex and nonlinear process. Battery performance, including the storage capacity and peak power, declines with increasing internal resistance inconsistency, imbalance of the internal battery heat and a series of side reactions [1]. If the performance of the batteries in an electric vehicle (EV) fails to meet the driving needs, then the battery should be replaced to meet driving mileage and safety requirements [2]. Due to the wide application of lithium-ion batteries in modern industry, including EVs, battery state-of-health (SoH) estimation has become an interesting and critical topic, and many methods have been presented in the past decade.

Since no consensus on SoH determination has been reached in industry or among scientists [3], different SoH estimation methods using different health indicators have been introduced in the literature. From the perspective of the health indicator adopted for SoH estimation, the features can be categorized into three groups: model fitted features, processed external features, and direct external features [1].

First, model fitted features, which are obtained based on curve fitting or online parameter identification algorithms, are used as health indicators. Then, the SoH is estimated by analyzing the correlation between each parameter and the SoH. Two types of parameters are obtained from different approaches. One type is obtained by open-circuit voltage (OCV) curve fitting [4], [5]. For instance, Ma *et al.* used the parameters obtained from Gaussian curve fitting to estimate the SoH based on a data-driven model. The results showed that the average relative errors of SoH estimation are less than 3% [4]. The other type is obtained from the terminal voltage curve combined with the equivalent circuit model [6]–[9]. For example, Bian *et al.* used the equivalent circuit model to describe the characteristics of the constant current part in the charging and discharging process of a lithium-ion battery. The least-square method was used to fit the charging curve and obtain the incremental capacity (IC) curve parameters for SoH estimation [7]. The advantage of this kind of method is that it is applicable to dynamic operating conditions. However, these methods are limited in that the model for simulating the battery working behavior and the process of model parameter identification have high storage and calculation requirements and thus are not well suited for real-time applications.

Second, processed external features are usually extracted from the differential charging curve under a constant current rate. Feature extraction [10]–[12], verification, and analysis are carried out on the curve under different aging conditions to establish the relationship between these health indicators and the SoH. According to the literature [10], [11], [13]–[19], feature extraction can be conducted on the IC/differential voltage (DV) or differential thermal voltammetry (DTV) curves. For instance, Li *et al.* established a quantitative relationship between the SoH and three peak-valley value points along with their positions on the IC curve fitted by a Gaussian process regression algorithm [13]. Additionally, the processed external features extracted from other curves, such as the charge/discharge curve and the OCV curve, can also be used for this kind of analysis [12], [20]–[24]. Liu el. constructed an online measurable health indicator, namely, the time interval of equal discharging voltage difference (TIEDVD), from the discharge curve for SoH estimation based on the UPF algorithm [23]. The advantage of this kind of method is that a small number of inputs is required for model training. However, the following disadvantages should be considered [1]:

1) Not suitable for dynamic operating conditions;

2) Constant current charge/discharge is required;

3) Some of the features can be hard to obtain during operation due to the limited capability of current battery management systems (BMSs).

Third, direct external features, such as the measured current, voltage, time, and temperature, are directly recorded by sensors in the BMS [19], [25]–[33]. For example, You *et al.* proposed a data-driven method for tracing the SoH by using BMS data such as the current, voltage, and temperature and their historical distributions [25]. Richardson *et al.* proposed a data-driven diagnostic technique, Gaussian process regression for in situ capacity estimation (GP-ICE), which estimates the battery capacity using voltage measurements over short periods of galvanostatic operation [27]. Xu *et al.* proposed a novel SoH estimation method based on the Wiener process

according to historical degradation data while considering the relaxation effect of lithium-ion batteries [19]. For this method, the features are easy to obtain from the BMS; thus, it is suitable or online applications. However, because the number of input features can be large, the computational cost is high.

During the literature review, we found a study on real-time SoH estimation based on the equivalent internal resistance (EIR). The equivalent internal resistance, as a significant electrical property parameter, is related to the temperature and SoH of the lithium-ion battery, and it decreases with the increase in temperature. When operating at a constant temperature, the EIR gradually increases with cycle aging. In addition, the trend of EIR with SoH is similar at different temperatures. Therefore, we propose to use the EIR to study the health status of batteries; battery sample cycling at a constant temperature of 40°C was used to verify the proposed method. The major contributions of this method are summarized as follows:

1) The relationship between the EIR and SoH is studied via experimentation and SoH modeling;

2) A fast EIR extraction method is proposed, and it can obtain the EIR in real time through a simple calculation;

3) A support vector regression (SVR)-based SoH estimation method with high precision and robustness is proposed, and it is demonstrated on a laboratory test dataset.

The remainder of this paper is organized as follows. Section 2 defines the problem and proposes the framework of this paper. Section 3 explains the SVR-based model and the fast EIR identification method. Section 4 analyzes the experimental results of the proposed method, and the accuracy and robustness are presented for the verification set. Finally, conclusions and future work are discussed in Section 5.

II. PROBLEM DEFINITION AND PROPOSED FRAMEWORK

Various factors, such as the temperature, test current, pressure, welding quality, and temperature inconsistency, affect battery degradation. Here, we summarize the main stress factors for battery design and operation/storage conditions [1], [34]–[36].

A. BATTERY DESIGN

The current collector design and welding quality, which corresponds to the connection between electrodes and the external circuit, have a large impact on cell temperature gradients and current density. Additionally, the stack pressure is relevant to the aging mechanisms since the electrodes will expand during cell operation within a constrained environment. Moreover, a resistance increase of the cell can be caused by the loss of electrical contact inside the porous electrode [34]. In this study, we assume that the influence of battery design can be neglected under ideal conditions.

B. OPERATION/STORAGE CONDITIONS

Battery degradation is affected by the environmental and operational conditions, such as ambient temperature,

charge/discharge current rate and cycling depth. When cells operate at high temperatures, transition metal dissolution is enhanced, while at low temperatures, lithium plating will lead to a loss of active material. High currents cause more heat waste, which will raise the battery temperature and accelerate battery aging. Battery aging is more influenced by high charge currents than by high discharge currents. In addition, Palacin *et al.* indicated that the electrode active material reversibility is more damaged when cells cycle at a higher depth of discharge (DoD) [34].

These factors are not linearly correlated, which complicates the extraction of correlations. However, these aging stress factors contribute to two main degradation phenomena [3]: loss of the storage capacity, which means a decrease in the maximum capacity of the battery for storing and supplying energy relative to that at the beginning of its life, and increase in impedance, which causes a decline in the available power provided by the battery. Therefore, SoH estimation must take into consideration both the capacity fade and impedance increase.

The capacity ratio, which reflects the loss of the storage capacity at the current moment, can be defined as follows:

$$S_{cap} = \frac{C_{now}}{C_{rated}} \times 100\% \tag{1}$$

where C_{rated} represents the rated capacity of the battery and C_{now} is the current maximum capacity of the battery.

The internal resistance ratio, which indicates the increase in impedance, can be described as follows:

$$S_R = \frac{R_{EOL} - R}{R_{EOL} - R_{new}} \times 100\% \tag{2}$$

where R_{EOL} represents the internal resistance at the end of battery life, R indicates the current internal resistance of the battery, and R_{new} is the internal resistance of the new battery.

Unfortunately, C_{now} is usually obtained based on the full charge-discharge process, which is difficult to operate in real-time applications. Likewise, obtaining R_{EOL} makes the battery unusable, which is clearly undesirable. Therefore, in this paper, regarding S_{cap} as the evaluation index of the SoH according to the IEEE standard [29], a real-time SoH estimation method is proposed that learns the relationship between S_{cap} and the EIR, which can be obtained in real time through a simple calculation. The framework of the proposed method is given as follows. First, an experimental study of the relationship between the SoH and EIR is conducted. Second, the EIR fast extraction principle and method are presented. Third, an SVR-based SoH estimation model is established.

III. SoH ESTIMATION METHOD
A. RELATIONSHIP BETWEEN THE SoH AND EIR STUDY

Since both capacity degradation and internal resistance can characterize the SoH, a correlation between the EIR and S_{cap} can be established as shown in (3):

$$S_{cap} = f(R) \tag{3}$$

Here, R represents a set of EIRs ($R_1, R_2, R_3, \ldots R_n$) at different states of charge (SoCs). Hence, a machine learning model can be established to describe the relationship between the SoH and vector R at the current moment. Then, the model can be employed in a BMS for online application.

B. EIR EXTRACTION OF THE SoC

Different SoHs are acquired based on data collection in a lithium-ion battery lifecycle test experiment [1], [37]–[39]. The correlation between the EIR and SoH can be described by the EIR spectrum, as shown in Figure 1.
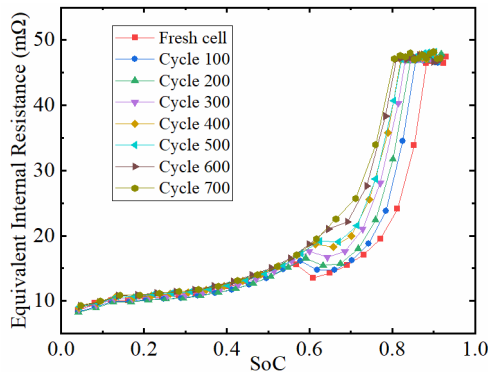
FIGURE 1. EIR changes with cycle aging for the battery (the EIRs are obtained through the charge evaluation process).

The EIR spectrum discussed above can be obtained through an internal resistance evaluation experiment at various battery SoHs, the process for which is shown in Figure 2. At the beginning of each internal resistance evaluation test process, we discharge the battery at a constant discharge current of 1/3C to the discharge cutoff voltage. Then, EIRs corresponding to different SoCs are obtained by alternately charging the battery for a period of time and shelving it.

Through the internal resistance evaluation test, the relationship between charging time and voltage can be obtained. A pictorial description of the internal resistance evaluation process is shown in Figure 3.

Let $U_{1i}(SoC)$ with $i = 1,2,3\ldots$, which represents the internal resistance evaluation number, denote the voltage at the last second of charging at a 0.5C current. Then, let $U_{2i}(SoC)$ denote the voltage at the last second of shelving at the same SoC as $U_{1i}(SoC)$ and I_{ci} represent a charge current of 0.5C. Therefore, the EIR as a function of the SoC is defined as follows:

$$R_i(SoC) = \left(\frac{|U_{2i}(SoC) - U_{1i}(SoC)|}{I_{ci}} \right) \quad (4)$$

The SoC can be expressed as:

$$SoC = \frac{\int_0^{t_i} I_{ci}(\tau)d\tau}{C_{now}} \times 100\% \quad (5)$$

where t_i indicates the charging process time until the current second τ and C_{now} represents the current maximum capacity, which can be obtained by emptying the battery. We can obtain
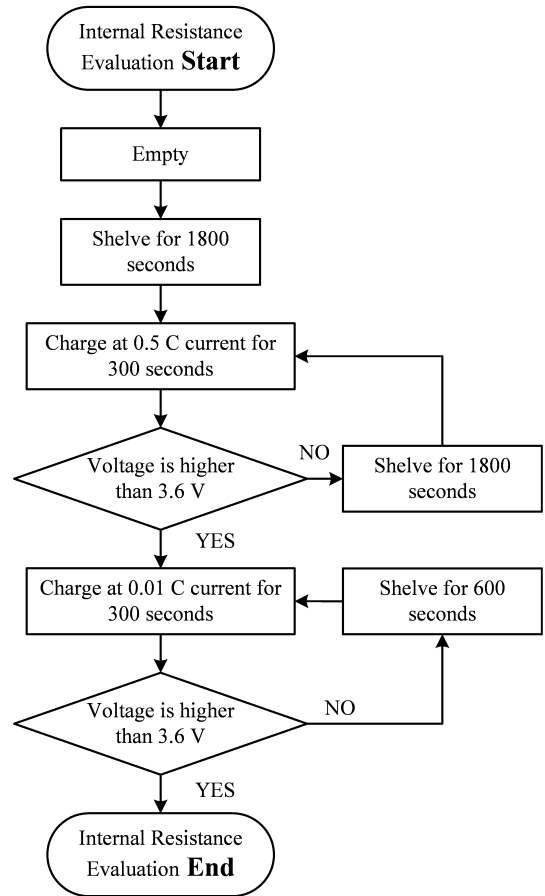

FIGURE 2. Flow chart of the internal equivalent resistance evaluation test process.
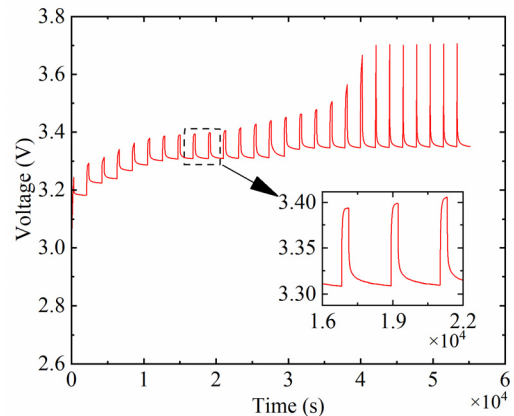

FIGURE 3. Pictorial description of the internal resistance evaluation process.

the EIR curve after all internal resistances at different SoCs are evaluated, as shown in Figure 4, and then we can obtain the cluster of resistance curves after multiple evaluations under different SoHs, as shown in Figure 1. The internal resistance of battery discharge is large when the SoC is less than 20% in the discharging process and more than 90% in
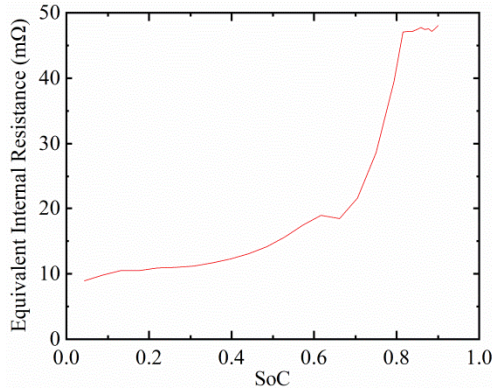
FIGURE 4. Pictorial description of the EIR at different SoCs (the EIRs are obtained through the charge evaluation process).

the charging process, resulting in an increase in the battery heat and large numerical fluctuations.

The range of charging and discharging of a battery is generally recommended to be 20%–90% [6].

To study the relationship between the evaluation number and EIRs corresponding to different SoCs, Figure 5 is obtained by taking the special abscissa intercept of all measurement points in the curve clusters in Figure 1, e.g., SoC = 0.6, with the abscissa as the evaluation number and the ordinate as the EIR value. Similarly, EIR curves corresponding to other SoCs can be obtained. Here, for visibility, not all evaluation curves are shown in Figure 1. Additionally, the relationship between the battery degradation level and the EIRs can be given by Equation (6):

$$S_{capi} = f(\mathbf{R}_i) \tag{6}$$

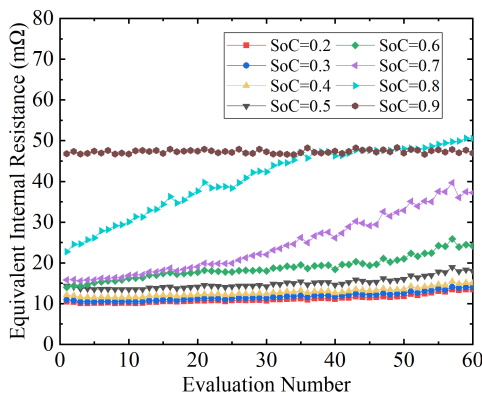where i represents the internal resistance evaluation number.

FIGURE 5. Relationship diagram between the battery degradation level and EIR.

C. SVR MODEL

SVR has the advantage of handling high-dimensional regression problems with limited training samples and restricted computation resources [40], [41]. An SVR-based method is developed in this paper for learning the relationship between the EIR and SoH.

For a given dataset $D = \{(\mathbf{x}_i, y_i), i = 1, 2, 3 \ldots\}$, let $\mathbf{x}_i = \mathbf{R}_i$ and $y_i = SoH_i$ be the input and output of the SVR model, where $\mathbf{R}_i$ represents the EIR vector and SoH_i is the *ith* SoH.

Assume that the regression plane is a nonlinear function:

$$f(x) = <\boldsymbol{\omega}, \quad \varphi(\mathbf{x}_i) > +b \tag{7}$$

where $\varphi(\cdot)$ is a nonlinear transformation that transforms the data into a higher dimensional feature space to perform linear separation. $\boldsymbol{\omega}$ and b are undetermined parameters.

Slack variables ξ_i and ξ_i^* are added to address infeasible constraints, and the loss function of the SVR model can be given by:

$$L = \min_{w,b,\xi_i\xi_i^*} \frac{1}{2}\|\mathbf{w}\|^2 + C\sum_{i=1}^{n}\left(\xi_i + \xi_i^*\right) \tag{8}$$

$$\text{subject to}: \begin{cases} f(\mathbf{x}_i) - y_i \leq \varepsilon + \xi_i \\ y_i - f(\mathbf{x}_i) \leq \varepsilon + \xi_i^* \\ \xi_i \geq 0 \ i = 1, 2, 3 \ldots, n \\ \xi_i^* \geq 0 \ i = 1, 2, 3 \ldots, n \end{cases} \tag{9}$$

We use the Lagrange function to solve the problem:

$$
\begin{aligned}
&L\left(w, b, \boldsymbol{\alpha}, \boldsymbol{\alpha}^*, \xi, \xi^*, \boldsymbol{\mu}, \boldsymbol{\mu}^*\right) \\
&= \frac{1}{2}\|\mathbf{w}\|^2 + C\sum_{i=1}^{n}\left(\xi_i + \xi_i^*\right) - \sum_{i=1}^{n}\mu_i\xi_i \\
&\quad - \sum_{i=1}^{n}\mu_i^*\xi_i^* + \sum_{i=1}^{n}\alpha_i\left(f(\mathbf{x}_i) - y_i - \varepsilon - \xi_i\right) \\
&\quad + \sum_{i=1}^{n}\alpha_i^*\left(y_i - f(\mathbf{x}_i) - \varepsilon - \xi_i^*\right)
\end{aligned} \tag{10}
$$

where $\boldsymbol{\alpha}, \boldsymbol{\alpha}^*, \boldsymbol{\mu}$, and $\boldsymbol{\mu}^*$ are the Lagrange multipliers, with $\alpha_i \geq 0, \alpha_i^* \geq 0, \mu_i \geq 0$, and $\mu_i^* \geq 0$.

According to (4), the SVR dual problem can be given as:

$$
\begin{aligned}
L = \max_{\boldsymbol{\alpha}\boldsymbol{\alpha}^*}\Big(&\sum_{i=1}^{n} y_i\left(\alpha_i^* - \alpha_i\right) - \varepsilon(\alpha_i^* + \alpha_i) \\
&- \frac{1}{2}\sum_{i=1}^{n}\sum_{j=1}^{n}\left(\alpha_i^* - \alpha_i\right)\left(\alpha_j^* - \alpha_j\right)\mathbf{x}_i^T\mathbf{x}_j
\end{aligned} \tag{11}
$$

$$\text{subject to}: \begin{cases} \sum_{i=1}^{n}\left(\alpha_i^* - \alpha_i\right) = 0 \\ 0 \leq \alpha_i, \alpha_i^* \leq C \end{cases} \tag{12}$$

According to the KKT condition:

$$
\begin{cases}
\alpha_i\left(f(\mathbf{x}_i) - y_i - \varepsilon - \xi_i\right) = 0 \\
\alpha_i^*\left(y_i - f(\mathbf{x}_i) - \varepsilon - \xi_i^*\right) = 0 \\
\quad (C - \alpha_i)\xi_i = 0 \\
\quad \left(C - \alpha_i^*\right)\xi_i^* = 0 \\
\quad \alpha_i\alpha_i^* = 0 \\
\quad \xi_i\xi_i^* = 0
\end{cases} \tag{13}
$$

The solution is given as follows:

$$f(x) = \sum_{i=1}^{m}\left(\alpha_i^* - \alpha_i\right)K(\mathbf{x}, \mathbf{x}_i) + b \tag{14}$$

where $K(\mathbf{x}, \mathbf{x}_i)$ represents the kernel function.

The common kernel functions are as follows:

$$K(x, x_i) = x \cdot x_i \tag{15}$$

$$K(x, x_i) = ((x \cdot x_i) + 1)^d \tag{16}$$

$$K(x, x_i) = e^{\left(-\frac{\|x - x_i\|^2}{\delta^2}\right)} \tag{17}$$

$$K(x, x_i) = \tanh(\varepsilon < x, x_i > +\theta) \tag{18}$$

They represent a linear kernel function, a polynomial kernel function, a Gaussian kernel function, and a sigmoid kernel function.

In this paper, we use the Gaussian kernel function $K(R, R_i)$ shown in Equation (18) to avoid a large amount of computation.

This optimization problem can be transformed into the dual problem, and its solution is given by:

$$f(x) = \sum_{i=1}^{m} (\alpha_i^* - \alpha_i) e^{\left(-\frac{\|x - x_i\|^2}{\delta^2}\right)} + b \tag{19}$$

D. HYPERPARAMETER OPTIMIZATION OF THE SVR MODEL

Since the accuracy and robustness of the models strongly depend on hyperparameter settings and default settings cannot guarantee optimal performance of machine learning techniques, the hyperparameters should be optimized [42]. The best model and corresponding hyperparameters are obtained by fine-tuning the structure, as shown in Figure 6. Since there are only two parameters, the computational time required to find the parameters via Gridsearch is not much longer than that by advanced methods [43]. Therefore, Gridsearch can be used as the optimizer and applied on the training set to update the hyperparameters. Moreover, K-fold cross-validation is used to evaluate performance, and it gives an excellent estimation of the generalization error, even on a small training set, according to Duan's research [44]. In this work, the evaluation index is the mean error of between observed and predicted values within the validation set. A diagram of the SoH estimation model from offline development to online prediction is shown in Figure 7.

IV. ESTIMATION RESULTS AND DISCUSSION

A. EXPERIMENTAL CONDITIONS AND SoH ESTIMATION

In this experiment, three 15 Ah lithium iron phosphate batteries were selected for the aging cycle experiment, as summarized in Table 1. More specifically, as shown in Figure 8, the aging cycle test was conducted at 40°C. In each aging cycle, the battery was charged and discharged at a constant rate in the set SoC range. After 20 cycles of the battery, a static capacity test was conducted to determine the maximum capacity of the battery under different health statuses, and an internal resistance test was conducted after 7200 seconds of shelving. The performance test program for the batteries is demonstrated in Figure 9.

In the experiment, the sensor error and the temperature difference of the programmable thermal chamber (KOMEG)
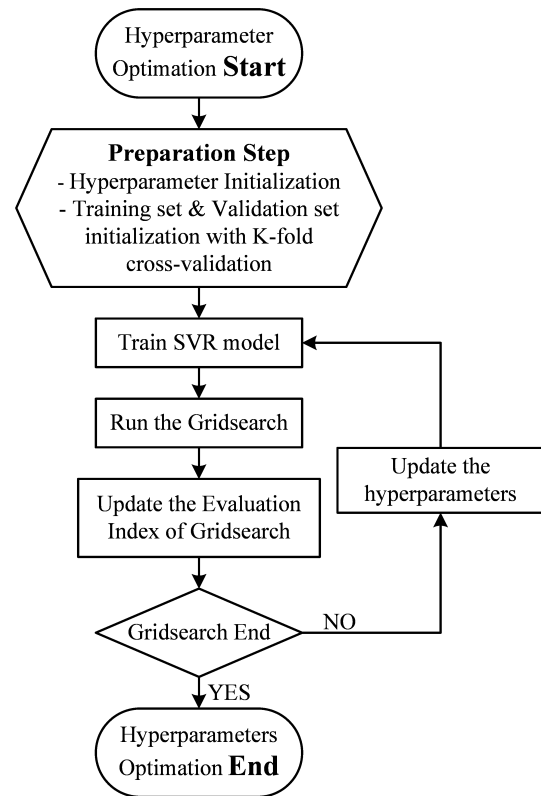

FIGURE 6. Fine-tuning process of hyperparameter optimization.

TABLE 1. Experimental conditions for battery degradation.

Temperature (°C)	Battery No.	SoC range	Charge-discharge rate
40°C	#01	0%-30%	1C
	#02	30%-60%	1C
	#03	60%-90%	1C

were less than 1°C. When constructing the SoH estimation model, we assumed that the cell temperature is uniform.

For SoH estimation, two batteries were taken as training samples to build the SVR model and determine the hyperparameters. Meanwhile, the other battery was applied to test the estimation accuracy of the proposed method. The battery test bench consisted of a battery charge-discharge tester, a programmable thermal chamber for temperature control and a host computer for data recording, as shown in Figure 10. In addition, the precisions of the voltage and current of the battery tester were less than 1 mV and 2 mA, respectively.

B. SoH ESTIMATION BY THE PROPOSED METHOD

In the obtained EIR spectrum, some representative EIRs in the SoC range from 20%–90% are selected as the inputs of the SVR model to reduce the algorithm running time [6].

To select the key EIRs for SVR modeling, quantitative analyses are critical. The Spearman correlation coefficient, generally expressed as ρ, is a measure of the correlation between two variables. The correlation coefficient determines
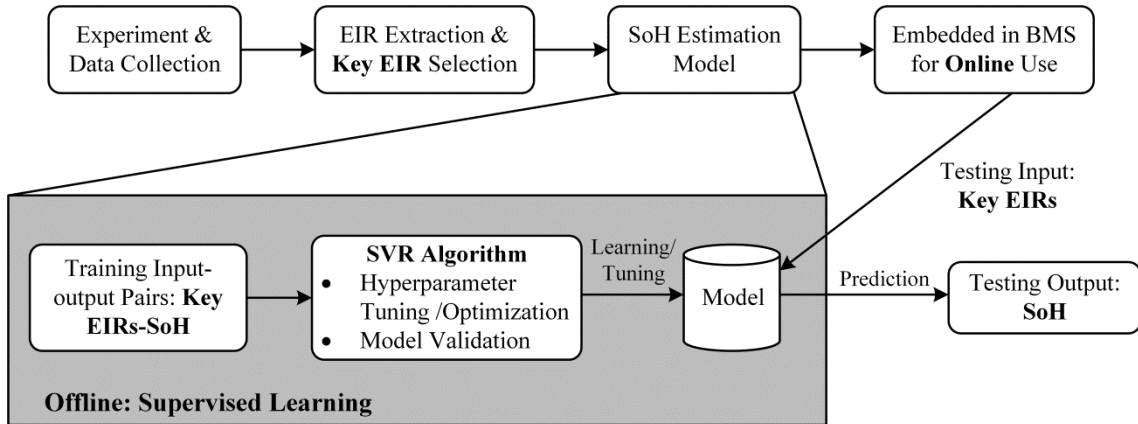
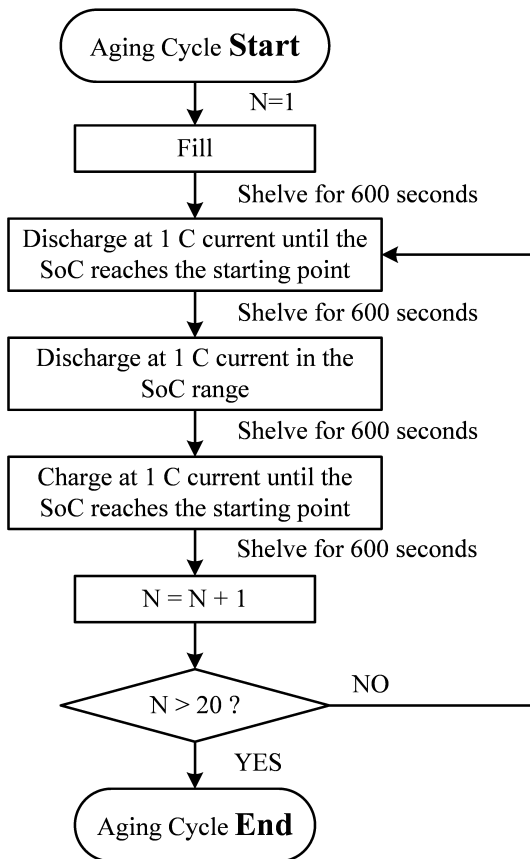**FIGURE 7.** Diagram of the concept of the SoH estimation model from offline development to online prediction.

FIGURE 8. Flow chart of the aging cycle test process.

FIGURE 9. Performance testing program for the batteries.

the importance of the two variables, which can be used to facilitate a rational selection of inputs.

Given two sets of random variables $F = \{F_1, F_2, \ldots\ldots, F_n\}$ and $G = \{G_1, G_2, \ldots\ldots, G_n\}$, where F_i and G_i are the *ith* elements in the sets, by sorting the elements in the two sets, we obtain two ranked sets $f = \{f_1, f_2, \ldots\ldots, f_n\}$ and $g = \{g_1, g_2, \ldots\ldots, g_n\}$. The element f_i is rank F_i in F, and f_i is rank G_i in G. The Spearman correlation coefficient of the
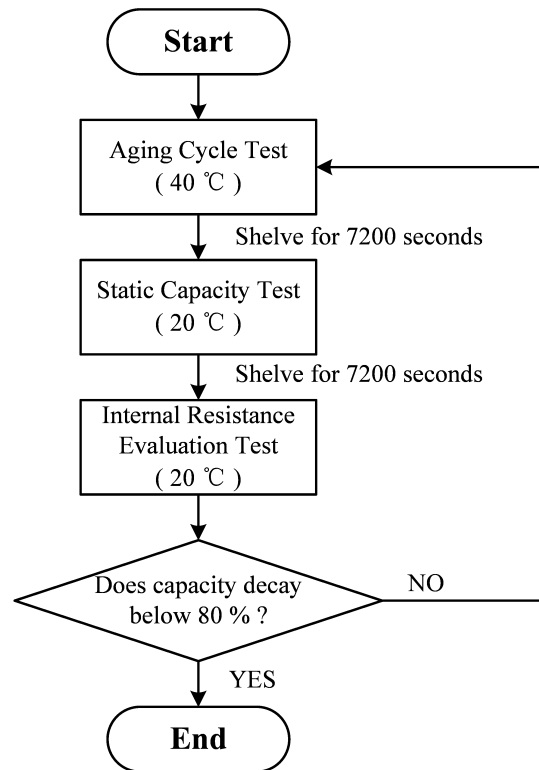
two sets F and G can be calculated using the ranked sets:

$$\rho = \frac{\sum_{i=1}^{N} (f_i - \bar{f})(g_i - \bar{g})}{\sqrt{\sum_{i=1}^{N} (f_i - \bar{f})^2 \sum_{i=1}^{N} (g_i - \bar{g})^2}} \qquad (20)$$

In Table 2, we list the Spearman correlation coefficients between the eight EIRs and the SoH for the three applied batteries. The EIRs with SoC $= 0.6, 0.7$ and 0.8 exhibit the three strongest correlations with the SoH. Therefore, we select these three EIRs as the training inputs to estimate the SoH.
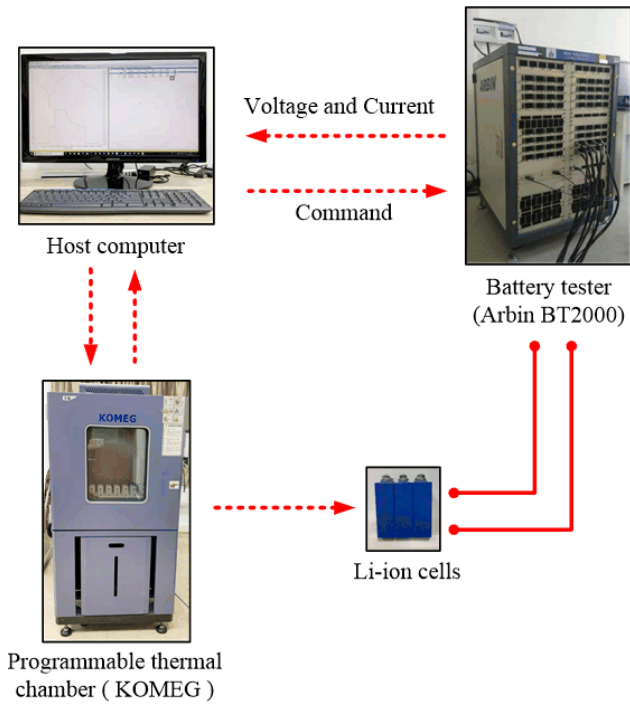
FIGURE 10. Diagram of the battery test bench.

**TABLE 2.** Results of spearman correlation coefficient analysis.

Battery No.	#01	#02	#03	Average
EIR (SoC=0.2)	0.9638	0.9794	0.8881	0.9438
EIR (SoC=0.3)	0.9742	0.9813	0.9209	0.9588
EIR (SoC=0.4)	0.9662	0.9708	0.9100	0.9490
EIR (SoC=0.5)	0.9414	0.9500	0.8922	0.9279
EIR (SoC=0.6)	0.9769	0.9906	0.9588	0.9754
EIR (SoC=0.7)	0.9896	0.9959	0.9934	0.9930
EIR (SoC=0.8)	0.9956	0.9951	0.9867	0.9925
EIR (SoC=0.9)	0.6262	0.2270	0.0775	0.3102

To yield the best performance, including the accuracy and computational cost of the method, the number of inputs of the SVR model is discussed in the remainder of this section.

First, the EIR corresponding to an SoC of 0.6 at different aging levels was taken as the input of the SVR model and recorded as R_{1n}. S_{capn}, the corresponding capacity ratio value, was taken as the evaluation indicator of the SVR model. The regression results and prediction results are given in Figure 11.

As shown in Figure 11, the regression and prediction results are barely satisfactory when one input is used for training. To improve the prediction accuracy, the EIRs corresponding to SoCs of 0.6 and 0.7 at different aging levels, namely, R_{1n} and R_{2n}, respectively, were taken as training inputs. The regression results and prediction results are shown in Figure 12.

After adding the second training input, the accuracy of regression and prediction is greatly improved. To further improve the accuracy, the EIR corresponding to an SoC of 0.8 at different aging levels, namely, R_{3n}, was also taken
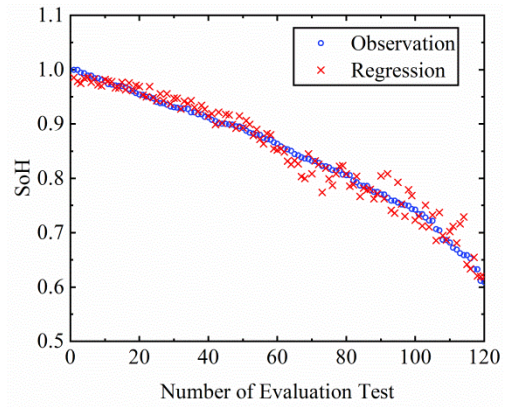
(a)
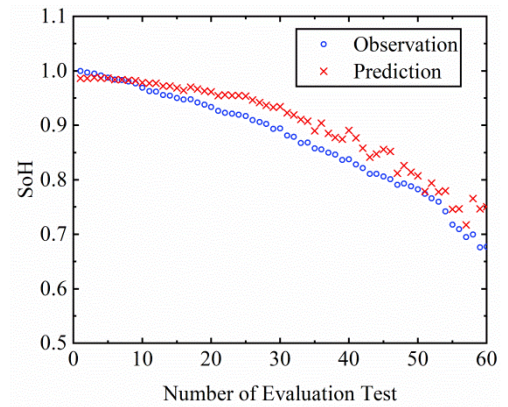
(b)

FIGURE 11. Regression and prediction results with one feature R_{1n} $(SoC = 0.6)$.

as an input of the SVR model. The regression results and prediction results are shown in Figure 13.

The hyperparameter optimization settings used in the SVR model in this work are given in Table 3. The mean error is minimized when C is equal to 10 and γ is equal to 0.1 for this problem.

**TABLE 3.** Hyperparameter optimization settings in the SVR model.

Hyperparameter	Type	Start	End	Learning rate
C	Numeric	2^{-5}	2^{12}	0.01
γ	Numeric	2^{-12}	2^3	0.01

The influences of different training indexes on the regression and prediction results are given in Table 4. The mean absolute error (MAE) and root mean square error (RMSE) were used as the performance indexes.

According to Table 4, when taking one input, for the EIR corresponding to an SoC of 0.6 at different aging levels, in the training model, the MAE evaluation indexes for regression and prediction were 0.0139 and 0.0293, respectively. In comparison, the MAE and RMSE of the regression decreased by more than 15%, and the MAE and RMSE of the prediction decreased by more than 9% when the number of
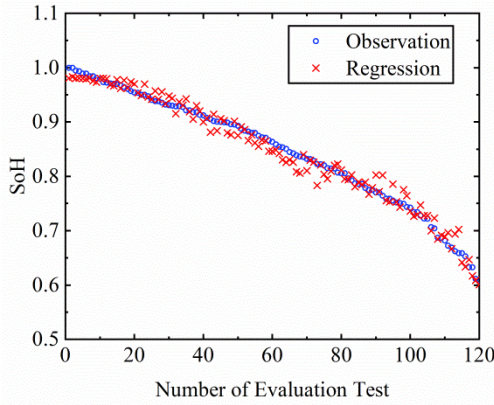
(a)
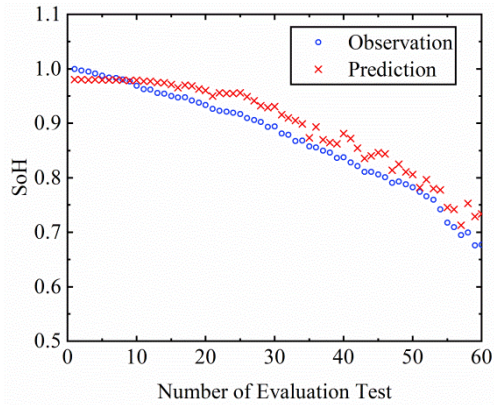
(b)

FIGURE 12. Regression and prediction results with two features R_{1n} $(SoC = 0.6)$ and R_{2n} $(SoC = 0.7)$.

TABLE 4. Results of different training indexes for regression and prediction.

Features	MAE		RMSE	
	Regression	Prediction	Regression	Prediction
R (SoC=0.6)	0.0139	0.0293	0.0183	0.0337
R (SoC=0.6) R (SoC=0.7)	0.0117	0.0265	0.0149	0.0293
R (SoC=0.6) R (SoC=0.7) R (SoC=0.8)	0.0116	0.0258	0.0143	0.0287

training inputs is increased to two. However, the improvement obtained by adding more training inputs is limited, as indicated by the results for an input number of three. That is, when the number of training inputs increases from one to two, the evaluation index RMSE significantly decreases. However, it slightly decreases when adding another input. Therefore, no more than three EIRs can describe the characteristics of battery aging. As shown in Figure 1 and Figure 5, the EIRs corresponding to an SoC of less than 0.57 or greater than 0.88 have little change in their degradation degrees. Therefore, the number of training inputs should be greater than one but at most three, and the SoCs corresponding to the respective EIRs should be greater than 0.57 and less than 0.88, considering the accuracy and operational efficiency.
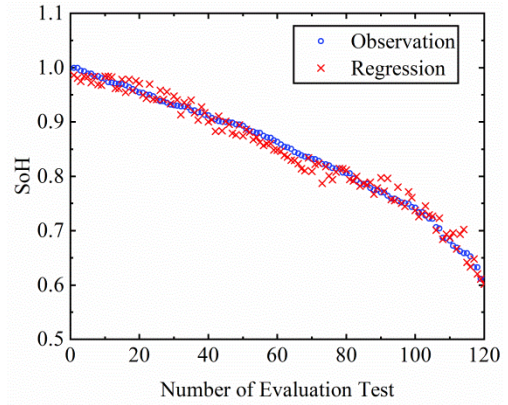
(a)
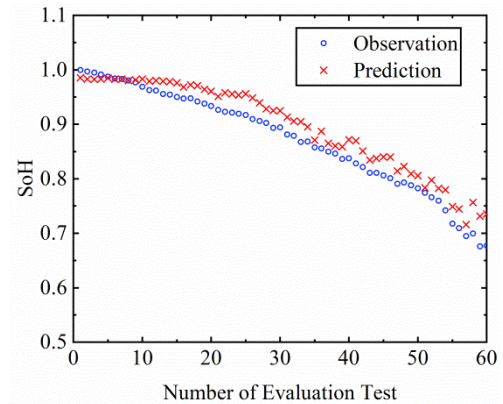
(b)

FIGURE 13. Regression and prediction results with three features R_{1n} $(SoC = 0.6)$, R_{2n} $(SoC = 0.7)$ and R_{3n} $(SoC = 0.8)$.

C. ROBUSTNESS OF THE PROPOSED METHOD

The measurement error of the BMS sensor in EVs will affect the SoH estimation. This section studies the robustness of the proposed method if measurement errors exist within the training data:

$$U'_{1i} = U_{1i} + e_{1i} \tag{21}$$

$$U'_{2i} = U_{2i} + e_{2i} \tag{22}$$

$$I'_{ci} = I_{ci} + e_{3i} \tag{23}$$

Here, U'_{2i} (i = 1,2,3...) is the charging OCV vector, e_{2i} is the measurement error, U'_{1i} (i = 1, 2, 3...) is the charging working voltage with measurement error e_{1i}, and I'_{ci} represents the current measured each time with measurement error e_{3i}.

The EIR and the SoC can be described as:

$$R'_i = \left(\frac{|U'_{2i} - U'_{1i}|}{I'_{ci}} \right) \tag{24}$$

$$SoC' = \frac{\int_0^{t_i} I'_{ci}(\tau)d\tau}{C_{now}} \times 100\% \tag{25}$$

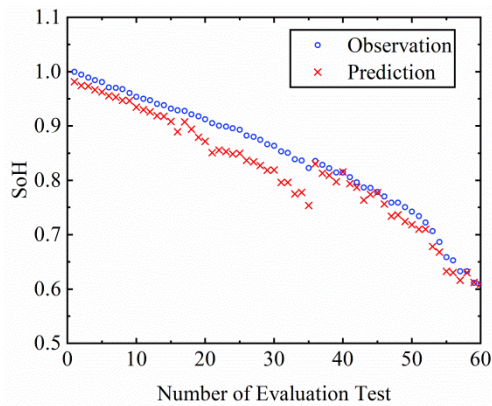To verify the robustness of the proposed method, we assume that the voltage detection of the sensor has a
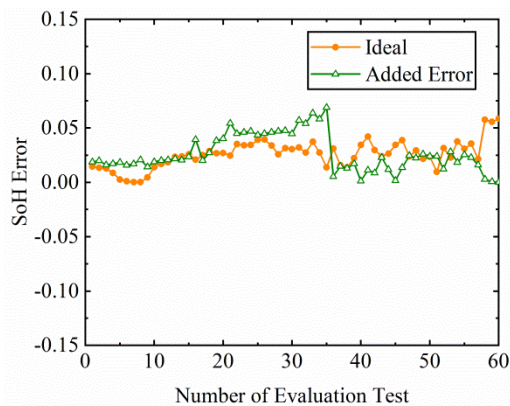
FIGURE 14. Prediction results after adding errors.

FIGURE 15. Error percentage of SoH estimation under ideal and added error conditions.

deviation of $\pm$ 5 mV, and the current has a deviation of $\pm$ 20 mA. The predicted results obtained by the proposed method are shown in Figure 14. The prediction accuracy decreases, and the results fluctuate to some extent after adding errors.

Comparing the ideal case with the case with errors, the error percentage can be obtained, as shown in Figure 15. The absolute value of the MAE percentage is at most 3%. This phenomenon precisely reflects the great robustness of the proposed method.

V. CONCLUSION

A novel SoH estimation method is illustrated in this paper. An SVR model has been employed based on the EIR according to the aging level of batteries. The EIR vector at various aging states has been obtained based on data collected in a lithium-ion battery lifecycle test experiment. A real-time EIR extraction approach in has been proposed to reduce the running time. In addition, we demonstrated that the accuracy of regression and prediction can be improved when two training inputs are utilized for the SVR model. The high robustness of the SoH estimation approach was validated by experimental results using training data with measurement errors. The simplicity of this method makes implementation for onboard

applications easy so that users can understand the state of the battery in EVs in a timely manner. However, the EIRs could change in actual use under complex working conditions. To further improve the robustness and accuracy, SoH prediction considering complex working conditions, such as the ambient temperature and current rate, is an important future research direction. Additionally, dynamic tests will be conducted to demonstrate its robustness and implementation.

REFERENCES

[1] Y. Li, K. Liu, A. M. Foley, A. Zülke, M. Berecibar, E. Nanini-Maury, J. Van Mierlo, and H. E. Hoster, "Data-driven health estimation and lifetime prediction of lithium-ion batteries: A review," *Renew. Sustain. Energy Rev.*, vol. 113, Oct. 2019, Art. no. 109254.

[2] K. W. E. Cheng, B. P. Divakar, H. Wu, K. Ding, and H. F. Ho, "Battery-management system (BMS) and SOC development for electrical vehicles," *IEEE Trans. Veh. Technol.*, vol. 60, no. 1, pp. 76–88, Jan. 2011.

[3] B. Maitane, "Accurate predictions of lithium-ion battery life," *Nature*, vol. 568, no. 7752, pp. 325–326, 2019.

[4] Z. Ma, R. Yang, and Z. Wang, "A novel data-model fusion state-of-health estimation approach for lithium-ion batteries," *Appl. Energy*, vol. 237, pp. 836–847, Mar. 2019.

[5] C. Weng, J. Sun, and H. Peng, "A unified open-circuit-voltage model of lithium-ion batteries for state-of-charge estimation and state-of-health monitoring," *J. Power Sources*, vol. 258, pp. 228–237, Jul. 2014.

[6] D. Yang, Y. Wang, R. Pan, R. Chen, and Z. Chen, "State-of-health estimation for the lithium-ion battery based on support vector regression," *Appl. Energy*, vol. 227, pp. 273–283, Oct. 2018.

[7] X. Bian, L. Liu, and J. Yan, "A model for state-of-health estimation of lithium ion batteries based on charging profiles," *Energy*, vol. 177, pp. 57–65, Jun. 2019.

[8] H. Pan, Z. Lü, H. Wang, H. Wei, and L. Chen, "Novel battery state-of-health online estimation method using multiple health indicators and an extreme learning machine," *Energy*, vol. 160, pp. 466–477, Oct. 2018.

[9] X. Li, Q. Wang, Y. Yang, and J. Kang, "Correlation between capacity loss and measurable parameters of lithium-ion batteries," *Int. J. Electr. Power Energy Syst.*, vol. 110, pp. 819–826, Sep. 2019.

[10] X. Li, Z. Wang, L. Zhang, C. Zou, and D. D. Dorrell, "State-of-health estimation for Li-ion batteries by combing the incremental capacity analysis method with grey relational analysis," *J. Power Sources*, vols. 410–411, pp. 106–114, Jan. 2019.

[11] X. Zheng and X. Deng, "State-of-health prediction for lithium-ion batteries with multiple Gaussian process regression model," *IEEE Access*, vol. 7, pp. 150383–150394, 2019.

[12] Y. Deng, H. Ying, E. Jiaqiang, H. Zhu, K. Wei, J. Chen, F. Zhang, and G. Liao, "Feature parameter extraction and intelligent estimation of the state-of-health of lithium-ion batteries," *Energy*, vol. 176, pp. 91–102, Jun. 2019.

[13] Y. Li, M. Abdel-Monem, R. Gopalakrishnan, M. Berecibar, E. Nanini-Maury, N. Omar, P. van den Bossche, and J. Van Mierlo, "A quick on-line state of health estimation method for li-ion battery with incremental capacity curves processed by Gaussian filter," *J. Power Sources*, vol. 373, pp. 40–53, Jan. 2018.

[14] Z. Wang, J. Ma, and L. Zhang, "State-of-Health estimation for lithium-ion batteries based on the multi-island genetic algorithm and the Gaussian process regression," *IEEE Access*, vol. 5, pp. 21286–21295, 2017.

[15] M. Berecibar, F. Devriendt, M. Dubarry, I. Villarreal, N. Omar, W. Verbeke, and J. Van Mierlo, "Online state of health estimation on NMC cells based on predictive analytics," *J. Power Sources*, vol. 320, pp. 239–250, Jul. 2016.

[16] H. Dai, G. Zhao, M. Lin, J. Wu, and G. Zheng, "A novel estimation method for the state of health of lithium-ion battery using prior knowledge-based neural network and Markov chain," *IEEE Trans. Ind. Electron.*, vol. 66, no. 10, pp. 7706–7716, Oct. 2019.

[17] C. Weng, J. Sun, and H. Peng, "Model parametrization and adaptation based on the invariance of support vectors with applications to battery State-of-Health monitoring," *IEEE Trans. Veh. Technol.*, vol. 64, no. 9, pp. 3908–3917, Sep. 2015.

[18] X. Feng, C. Weng, X. He, X. Han, L. Lu, D. Ren, and M. Ouyang, "Online state-of-health estimation for Li-ion battery using partial charging segment based on support vector machine," *IEEE Trans. Veh. Technol.*, vol. 68, no. 9, pp. 8583–8592, Sep. 2019.

[19] X. Xu, C. Yu, S. Tang, X. Sun, X. Si, and L. Wu, "State-of-health estimation for lithium-ion batteries based on Wiener process with modeling the relaxation effect," *IEEE Access*, vol. 7, pp. 105186–105201, 2019.

[20] K. Honkura, K. Takahashi, and T. Horiba, "Capacity-fading prediction of lithium-ion batteries based on discharge curves analysis," *J. Power Sources*, vol. 196, no. 23, pp. 10141–10147, Dec. 2011.

[21] I. Bloom, B. W. Cole, J. J. Sohn, S. A. Jones, E. G. Polzin, V. S. Battaglia, G. L. Henriksen, C. Motloch, R. Richardson, T. Unkelhaeuser, D. Ingersoll, and H. L. Case, "An accelerated calendar and cycle life study of Li-ion cells," *J. Power Sources*, vol. 101, no. 2, pp. 238–247, Oct. 2001.

[22] T. Wang, L. Pei, T. Wang, R. Lu, and C. Zhu, "Capacity-loss diagnostic and life-time prediction in lithium-ion batteries: Part 1. Development of a capacity-loss diagnostic method based on open-circuit voltage analysis," *J. Power Sources*, vol. 301, pp. 187–193, Jan. 2016.

[23] D. Liu, X. Yin, Y. Song, W. Liu, and Y. Peng, "An on-line state of health estimation of lithium-ion battery using unscented particle filter," *IEEE Access*, vol. 6, pp. 40990–41001, 2018.

[24] J. Kim, H. Chun, M. Kim, J. Yu, K. Kim, T. Kim, and S. Han, "Data-driven state of health estimation of li-ion batteries with RPT-reduced experimental data," *IEEE Access*, vol. 7, pp. 106987–106997, 2019.

[25] G.-W. You, S. Park, and D. Oh, "Real-time state-of-health estimation for electric vehicle batteries: A data-driven approach," *Appl. Energy*, vol. 176, pp. 92–103, Aug. 2016.

[26] Y. Li, C. Zou, M. Berecibar, E. Nanini-Maury, J. C.-W. Chan, P. van den Bossche, J. Van Mierlo, and N. Omar, "Random forest regression for online capacity estimation of lithium-ion batteries," *Appl. Energy*, vol. 232, pp. 197–210, Dec. 2018.

[27] R. R. Richardson, C. R. Birkl, M. A. Osborne, and D. A. Howey, "Gaussian process regression for *in situ* capacity estimation of lithium-ion batteries," *IEEE Trans Ind. Informat.*, vol. 15, no. 1, pp. 127–138, Jan. 2019.

[28] A. Eddahech, O. Briat, N. Bertrand, J.-Y. Delétage, and J.-M. Vinassa, "Behavior and state-of-health monitoring of li-ion batteries using impedance spectroscopy and recurrent neural networks," *Int. J. Electr. Power Energy Syst.*, vol. 42, no. 1, pp. 487–494, Nov. 2012.

[29] Z. Min, H. Wensong, and N. C. Kar, "The SOH estimation of LiFePO₄ battery based on internal resistance with Grey Markov Chain," in *Proc. ITEC*, Dearborn, MI, USA, 2016, pp. 1–6.

[30] V. Klass, M. Behm, and G. Lindbergh, "A support vector machine-based state-of-health estimation method for lithium-ion batteries under electric vehicle operation," *J. Power Sources*, vol. 270, pp. 262–272, Dec. 2014.

[31] S. Tang, C. Yu, X. Wang, X. Guo, and X. Si, "Remaining useful life prediction of lithium-ion batteries based on the Wiener process with measurement error," *Energies*, vol. 7, no. 2, pp. 520–547, Feb. 2014.

[32] X.-S. Si, "An adaptive prognostic approach via nonlinear degradation modeling: Application to battery data," *IEEE Trans. Ind. Electron.*, vol. 62, no. 8, pp. 5082–5096, Aug. 2015.

[33] J. Yu, "Health degradation detection and monitoring of lithium-ion battery based on adaptive learning method," *IEEE Trans. Instrum. Meas.*, vol. 63, no. 7, pp. 1709–1721, Jul. 2014.

[34] M. R. Palacín, "Understanding ageing in li-ion batteries: A chemical issue," *Chem. Soc. Rev.*, vol. 47, no. 13, pp. 4924–4933, 2018.

[35] J. Vetter, P. Novák, M. R. Wagner, C. Veit, K.-C. Möller, J. O. Besenhard, M. Winter, M. Wohlfahrt-Mehrens, C. Vogler, and A. Hammouche, "Ageing mechanisms in lithium-ion batteries," *J. Power Sources*, vol. 147, nos. 1–2, pp. 269–281, 2005.

[36] C. R. Birkl, M. R. Roberts, E. McTurk, P. G. Bruce, and D. A. Howey, "Degradation diagnostics for lithium ion cells," *J. Power Sources*, vol. 341, pp. 373–386, Feb. 2017.

[37] E. Sarasketa-Zabala, E. Martinez-Laserna, M. Berecibar, I. Gandiaga, L. M. Rodriguez-Martinez, and I. Villarreal, "Realistic lifetime prediction approach for Li-ion batteries," *Appl. Energy*, vol. 162, pp. 839–852, Jan. 2016.

[38] A. Nuhic, T. Terzimehic, T. Soczka-Guth, M. Buchholz, and K. Dietmayer, "Health diagnosis and remaining useful life prognostics of lithium-ion batteries using data-driven methods," *J. Power Sources*, vol. 239, pp. 680–688, Oct. 2013.

[39] Y. Zhou, M. Huang, Y. Chen, and Y. Tao, "A novel health indicator for on-line lithium-ion batteries remaining useful life prediction," *J. Power Sources*, vol. 321, pp. 1–10, Jul. 2016.

[40] A. J. Smola and B. Schölkopf, "A tutorial on support vector regression," *Statist. Comput.*, vol. 14, no. 3, pp. 199–222, Aug. 2004.

[41] L. Li and Y. Duan, "Notice of Retraction: A GA-based feature selection and parameters optimization for support vector regression," in *Proc. ICNC*, Shanghai, China, 2011, pp. 335–339.

[42] P. Schratz, J. Muenchow, E. Iturritxa, J. Richter, and A. Brenning, "Hyperparameter tuning and performance assessment of statistical and machine-learning algorithms using spatial data," *Ecol. Model.*, vol. 406, pp. 109–120, Aug. 2019.

[43] S. Mezzatesta, C. Torino, P. D. Meo, G. Fiumara, and A. Vilasi, "A machine learning-based approach for predicting the outbreak of cardiovascular diseases in patients on dialysis," *Comput. Methods Programs Biomed.*, vol. 177, pp. 9–15, Aug. 2019.

[44] K. Duan, S. S. Keerthi, and A. N. Poo, "Evaluation of simple performance measures for tuning SVM hyperparameters," *Neurocomputing*, vol. 51, pp. 41–59, Apr. 2003.

XIAOJUN TAN received the Ph.D. degree from Sun Yat-sen University, China, in 2005. He was a Lecturer with the Engineering School, Sun Yat-sen University, from 2005 to 2010, and also an Associate Professor, from 2010 to 2017. Since 2010, he has been a Chief Engineer with the Electric Vehicle Research Center, Dongguan-SYSU Institute. He is currently an Associate Professor with the School of Intelligent Systems Engineering. His research interests include computer vision, control networks, smart driving, and battery management systems.

YUQING TAN received the B.E. degree in traffic engineering from Sun Yat-sen University, in 2017, where she is currently pursuing the M.E. degree in transportation engineering with the School of Intelligent Systems Engineering. Her research interests include battery management systems, machine learning, and deep learning.
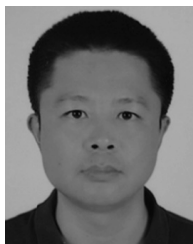
DI ZHAN received the B.E. degree from Sun Yat-sen University, in 2018, where she is currently pursuing the M.E. degree in transportation engineering with the School of Intelligent Systems Engineering. Her research interests include battery energy management and control strategy of electric vehicle.

ZE YU received the B.E. and M.E. degrees in automotive engineering from Chang'an University, China, in 2012 and 2016, respectively. He is currently pursuing the Ph.D. degree with the School of Intelligent Systems Engineering, Sun Yat-sen University. His research interests include artificial intelligence, deep learning, and intelligent vehicles.

YUQIAN FAN received the B.E. degree in communication engineering from Harbin Engineering University, China, in 2009, and the M.E. degree in electronics and communication engineering form Wuhan University, China, in 2011. He is currently pursuing the Ph.D. degree in intelligent transportation engineering with Sun Yat-sen University. His research interests include battery aging model, battery thermal management, and control strategy.

JUN LI received the Ph.D. degree in microelectronics and solid-state electronics from the Shanghai Advanced Research Institute, Chinese Academy of Sciences. He was a Senior Engineer with Huawei, China, from 2016 to 2017. He is currently an Associate Researcher with the School of Intelligent Systems Engineering, Sun Yat-sen University. His research interests include the system integration and application of fuel cells and lithium-ion battery.

• • •

JIANZHI QIU received the B.E. degree in traffic engineering from Sun Yat-sen University, in 2017, where he is currently pursuing the M.E. degree with the School of Intelligent Systems Engineering. His research interests include battery management systems, machine learning, and deep learning.